Quantum decoherence versus classical depolarization in nanohole arrays

Altewischer, E.; Oei, Y.C.; Exter, M.P. van; Woerdman, J.P.

Quantum decoherence versus classical depolarization in nanohole arrays

E. Altewischer, Y. C. Oei, M. P. van Exter, and J. P. Woerdman
Huygens Laboratory, Leiden University, P.O. Box 9504, 2300 RA Leiden, The Netherlands
(Received 11 January 2005; published 21 July 2005)

We present a theoretical model of the quantum decoherence experienced by a pair of polarization-entangled photons, after one of them is sent through a nanohole array, and compare this with the classical depolarization experienced by light with a fixed polarization when this is sent through the same array. We discuss the conditions under which the quantum visibility and the classical degree of polarization are the same. Experimental verification is done with arrays of square and hexagonal symmetry.

DOI: 10.1103/PhysRevA.72.013817 PACS number(s): 42.50.Dv, 42.25.Ja, 73.20.Mf, 78.67.−n

I. INTRODUCTION

Since the first experiment that demonstrated the extraordinary transmission of metal nanohole arrays [1], a number of studies have stressed the importance of the optical polarization and its relation to surface plasmon (SP) propagation [2–7]. These issues show up most prominently if the array is illuminated with a strongly focused beam, since in this case the coupling of the SP propagation to the incident polarization leads to spatial nonuniformities. In a previous experiment the hole-array transmission was probed with single photons out of polarization-entangled photon pairs [8], i.e., with pairs where the polarization of each photon is *undetermined*, but quantum correlated to the other photon in the pair. This experiment showed that the entanglement could be fully transferred to the excited SPs for plane-wave illumination, but that quantum decoherence occurred for focused illumination (where the focal spot is still covering many holes).

In this paper we address the fundamental question how this observed quantum decoherence is related to the classical depolarization experienced by light with a *fully determined* polarization that passes through the nanohole array in an identical configuration. This distinction between *undetermined* and *determined* lies at the heart of quantum measurement theory and the interpretation of the projection postulate. Although a theoretical description of the quantum experiment has already been given in Ref. [9], we consider that description too complicated for practical use. Furthermore, there are several subtleties involved that took us some time to resolve experimentally. We will discuss the conditions under which both the classical depolarization and the quantum decoherence can be simply expressed in the angle- and polarization-dependent transmission ("transfer function") of the hole array. Note that this description in terms of a transfer function does not depend on the details of the transmission process and is completely general in that respect. We present data for both the classical and the quantum experiments and compare these, for square as well as for hexagonal arrays. Special attention is given to an averaging procedure that allows one to remove spurious effects of linear anisotropies in practical hole arrays (see Appendix).

II. THEORETICAL COMPARISON OF CLASSICAL DEPOLARIZATION AND QUANTUM DECOHERENCE

We start our theoretical description of classical depolarization by recapitulating the transmission properties of a hole array in the paraxial limit. Restricting ourselves to the zeroth-order diffraction, these properties can be fully captured in a 2×2 transfer matrix $t(\vec{\theta},\omega)$, which relates the optical input field at angle of incidence $\vec{\theta}$ and frequency ω to the output field at the same angle and frequency:

$$\vec{E}_{out}(\vec{\theta},\omega)=t(\vec{\theta},\omega)\vec{E}_{in}(\vec{\theta},\omega). \tag{1}$$

Depolarization can occur when an array is illuminated with a wide-angle beam and the transfer matrix also shows a combined angular and polarization dependence, producing different output polarizations for the same input polarization at different angles of incidence. This process can be fully quantified by measuring the (4×4) Mueller matrix, which relates the spatially averaged input to output polarizations via Stokes vectors [10,11].

For perfectly square and hexagonal hole arrays the Mueller matrix is diagonal [7,12], with elements M_{ii} $(i=0, 1, 2, 3)$, and it suffices to express the depolarization by the three numbers $\Pi_i \equiv M_{ii}/M_{00}$. These quantities are equal to the degree of polarization $(\mathcal{D})$ [10,11] of the output light of the array for linear input polarization along 0° (corresponding to $i=1$) and 45° $(i=2)$, and circular input polarization $\sigma^+(i=3)$, respectively; M_{00} is the transmitted power for unpolarized input light. In practice, off-diagonal elements of the Mueller matrix cannot always be neglected due to array imperfections [7]. However, even in this case, the Π_i remain useful to characterize the polarization behavior of such arrays, provided that the off-diagonal elements are small compared to the diagonal elements. The Π_i are approximately equal to the average of the $\mathcal{D}$'s of the output light of the array for input polarizations corresponding to i and to its orthogonal direction, respectively (see Appendix); therefore we can use the term $\mathcal{D}$ for Π_i also in the case of slightly nonperfect arrays.

The degrees of polarization Π_i can be determined experimentally with the setup shown in Fig. 1. Here a hole array is illuminated with light of a given spectral and angular bandwidth, where the latter is set by a lens, with focal length f, plus a diaphragm. To determine the $\mathcal{D}$, we use an averaging procedure conforming to the discussion above, where for each i two input polarizations are prepared, one corresponding to i and one to its orthogonal direction. Subsequently, for each input polarization, the power of the output beam $P_{\parallel}$ and $P_{\perp}$ is measured for settings of the analyzer parallel and per-

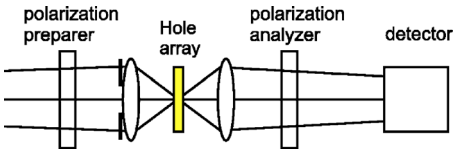

FIG. 1. (Color online) The setup used for the classical polarization experiment, with the source a Ti:sapphire laser at 813 nm wavelength (on the left, not shown). The input polarization state is prepared by a combination of polarizer and half-wave plate, and analyzed with a polarizer. The hole array is centered inside the confocal one-to-one telescope.

pendicular to the preparer, respectively. The Π_i is then computed from

$$\Pi_i = \frac{P_{\parallel}^{av} - P_{\perp}^{av}}{P_{\parallel}^{av} + P_{\perp}^{av}}, \tag{2}$$

where each quantity is the average over the two orthogonal input polarizations. In this paper, we will concentrate on two specific choices for the input polarization, namely 0° and 45°. By expressing the optical fields in terms of Stokes parameters and using the fact that the incident field is transformed by the hole array via

$$E(\vec{\theta},\omega)\vec{e}_H \rightarrow t_{HH}(\vec{\theta},\omega)E(\vec{\theta},\omega)\vec{e}_H + t_{VH}(\vec{\theta},\omega)E(\vec{\theta},\omega)\vec{e}_V, \tag{3}$$

one can express the degree of polarization Π in terms of the input field and the elements of the transmission matrix t as

$$\Pi_{0^\circ} = \frac{\langle\langle(|t_{HH}|^2 - |t_{VH}|^2 + |t_{VV}|^2 - |t_{HV}|^2)|E|^2\rangle\rangle}{\langle\langle(|t_{HH}|^2 + |t_{VH}|^2 + |t_{VV}|^2 + |t_{HV}|^2)|E|^2\rangle\rangle}, \tag{4a}$$

$$\Pi_{45^\circ} = \frac{\langle\langle 2\mathrm{Re}\{t_{HH}t_{VV}^* + t_{VH}t_{HV}^*\}|E|^2\rangle\rangle}{\langle\langle(|t_{HH}|^2 + |t_{VH}|^2 + |t_{VV}|^2 + |t_{HV}|^2)|E|^2\rangle\rangle}. \tag{4b}$$

Here the double brackets denote the integration over all angles and frequencies contained in the beam, and the input intensity $|E|^2$ should have identical angular and spectral distributions for each of the four measurements.

Although Eqs. (4a) and (4b) are strictly valid, their relation to the experimental configuration of Fig. 1 is straightforward only if the illumination has sufficient spatial coherence. This is a valid assumption if the illumination of the telescope-input lens has a negligible wave-vector spread; alternatively, this assumption can be formulated in terms of the size of the focus inside the telescope: this has to be much smaller than the beam size on the telescope lenses, as can be seen from ray-optics arguments. Under this condition the internal angle $\vec{\theta}$ inside the telescope can be mapped one-to-one to the transverse position $\vec{r}$ on the input lens via $\vec{\theta}=-\vec{r}/f$. Assuming this makes our description much simpler than that of Ref. [9]; we consider the angle-dependent transmission of the hole array $t(\vec{\theta},\omega)$, which in Ref. [9] is denoted by $\mathbb{F}(\vec{q}_2)$, to be the only physically relevant quantity.

The quantum decoherence experienced by polarization-entangled photons depends on the biphoton state or amplitude function, just as the classical depolarization depends on the (one-photon) field E. Most descriptions of polarization-entangled photons start from the biphoton state:

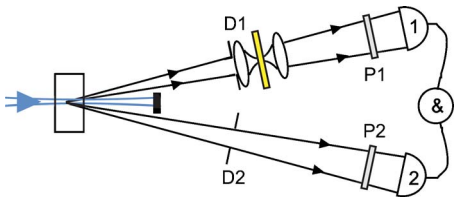

FIG. 2. (Color online) The SPDC setup used in the quantum experiment, with the source a nonlinear BBO crystal plus the standard compensation scheme of half-wave plate and compensating crystals (not shown in detail). The hole arrays are placed inside the confocal telescope in one of the beams.

$$|\psi\rangle = \frac{1}{\sqrt{2}}(|H_1V_2\rangle + e^{i\alpha}|V_1H_2\rangle), \tag{5}$$

where the two photons, with horizontal and vertical polarizations, travel along directions labeled by 1 and 2. For instance, in the standard type-II spontaneous parametric down conversion (SPDC) setup, as shown in Fig. 2, a nonlinear crystal is able to convert an incident pump photon to two orthogonally polarized photons at the double wavelength, which are emitted along two intersecting cones. At the exact crossings of these cones the polarization of the individual photons is undetermined, and Eq. (5) correctly describes the polarization properties of the biphoton state if the spatial and frequency selection is sufficiently narrow. In an experiment, this state can only be produced approximately, because the photons can also be labeled by their frequency and wave vector. Both of these have to be taken into account because a practical detector will measure a finite part of the crossings, set by the apertures in Fig. 2, within a finite frequency window. In this case, the paraxially exact SPDC state behind the apertures at the ring crossings can be written as

$$\begin{aligned}|\psi\rangle = \int d\vec{q}_1 d\vec{q}_2 d\omega_1 d\omega_2 [&\Phi_{HV}(\vec{q}_1,\omega_1;\vec{q}_2,\omega_2) \\ &\times|H,\vec{q}_1,\omega_1;V,\vec{q}_2,\omega_2\rangle + \Phi_{VH}(\vec{q}_1,\omega_1;\vec{q}_2,\omega_2) \\ &\times|V,\vec{q}_1,\omega_1;H,\vec{q}_2,\omega_2\rangle],\end{aligned} \tag{6}$$

showing explicitly the wave vector $\vec{q}$ and frequency ω dependent (two-photon) amplitude functions Φ_{ij} $(i,j=H,V)$ for each of the two-photon combinations [13]. The integration is over the angular area contained in the apertures and the frequency window of the detectors.

A simple experimental measure for the degree of entanglement can be obtained from the two-photon fringe visibility:

$$V_{\varphi_1} \equiv \frac{R_{max}^{av} - R_{min}^{av}}{R_{max}^{av} + R_{min}^{av}}, \tag{7}$$

which can take values between 0 and 1. It is measured in the setup of Fig. 2 by setting the transmission axis of one of the polarizers at the appropriate φ_1 and $\varphi_1+\pi/2$, respectively, and measuring in each case the maximum and minimum coincidence rates R_{max} and R_{min} at the corresponding settings of

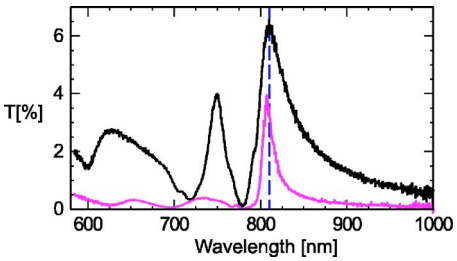

FIG. 3. (Color online) Transmission spectra under almost plane-wave illumination at normal incidence for the square (black curve) and hexagonal array (gray curve). The dashed vertical line indicates the resonance wavelength of 813 nm used in the experiments.

the second polarizer. By defining the visibility V in terms of the coincidence rates R_{av} averaged over the two input settings the visibility becomes more robust against imperfections of the hole array that will be considered below, in a manner analogous to the discussion above for the $\mathcal{D}\ \Pi_i$.

For a type-II SPDC source, producing the state $|\psi\rangle$ of Eq. (6), the visibility in the linear polarization basis oriented at 0° with respect to the crystal axes (along H and V) is always 1 because there is no interference between Φ_{HV} and Φ_{VH} in this case. The visibility along 45°, however, is given by

$$V_{45^\circ} = \frac{\langle\langle 2\mathrm{Re}(\Phi_{HV}\Phi_{VH}^{*})\rangle\rangle}{\langle\langle|\Phi_{HV}|^2 + |\Phi_{VH}|^2\rangle\rangle}, \tag{8}$$

where the brackets denote the integration over $\vec{q}$ and ω. Therefore the source produces perfectly polarization-entangled photons ($V_{45^\circ}=1$) only if Φ_{HV} and Φ_{VH} are identical within the considered angular and frequency bandwidths. This is the case for either an infinitely thin crystal or a properly corrected thick crystal [14], followed by detection within sufficiently small angular and frequency windows. Note that the overlap integral of Φ_{HV} and Φ_{VH} in the numerator has the shape of a coherence function, so that two perfectly entangled photons can be considered to be mutually fully coherent (within the considered angular and spectral bandwidths). This two-photon coherence is independent of the one-photon coherence of each of the beams separately; in fact, the one-photon properties of a SPDC source are indistinguishable from those of a thermal source with identical bandwidths [15].

By putting a hole array (with transmission matrix t) at the focus of a confocal telescope in beam 1 of the SPDC setup (see Fig. 2) the SPDC state is changed in the following way:

$$\int d\,\vec{q}_{1,2}d\omega_{1,2}\Phi_{HV}|H,\vec{q}_1,\omega_1;V,\vec{q}_2,\omega_2\rangle$$

$$\rightarrow \int d\,\vec{q}_{1,2}d\omega_{1,2}\Phi_{HV}\{t_{HH}(\vec{\theta}_1,\omega_1)|H,\vec{q}_1,\omega_1;V,\vec{q}_2,\omega_2\rangle$$

$$+ t_{VH}(\vec{\theta}_1,\omega_1)|V,\vec{q}_1,\omega_1;V,\vec{q}_2,\omega_2\rangle\}, \tag{9}$$

and analogously for the $|VH\rangle$ term. We again assume "sufficient spatial coherence" and, additionally, that the telescope input lens is in the far field of the source. This allows us to relate the angle inside the telescope $\vec{\theta}$ to the transverse momentum of the photon $\vec{q}$ as $\vec{\theta}_1=-L\vec{q}_1/(fk)$, where $L\gg f$ is the distance from the input lens to the source and $k=2\pi/\lambda$. Because the hole array can create additional $|HH\rangle$ and $|VV\rangle$ terms, the visibilities observed behind the hole array (see Fig. 2) are given by

$$V_{0^\circ} = \frac{\langle\langle(|t_{HH}|^2 - |t_{VH}|^2)|\Phi_{HV}|^2 + (|t_{VV}|^2 - |t_{HV}|^2)|\Phi_{VH}|^2\rangle\rangle}{\langle\langle(|t_{HH}|^2 + |t_{VH}|^2)|\Phi_{HV}|^2 + (|t_{VV}|^2 + |t_{HV}|^2)|\Phi_{VH}|^2\rangle\rangle}, \tag{10a}$$

$$V_{45^\circ} = \frac{\langle\langle 2\mathrm{Re}\{\Phi_{HV}\Phi_{VH}^{*}(t_{HH}t_{VV}^{*} + t_{VH}t_{HV}^{*})\}\rangle\rangle}{\langle\langle(|t_{HH}|^2 + |t_{VH}|^2)|\Phi_{HV}|^2 + (|t_{VV}|^2 + |t_{HV}|^2)|\Phi_{VH}|^2\rangle\rangle}. \tag{10b}$$

If we now compare Eqs. (4a), (4b), (10a), and (10b), we see that for perfectly entangled photons, i.e., $\Phi_{HV}=\Phi_{VH}=\Phi$, the input one-photon distribution $|E|^2$ in the classical experiment and the two-photon distribution $|\Phi|^2$ in the quantum experiment play the same role, i.e., $\Pi_i=V_i$ if $|E|^2=|\Phi|^2$. We repeat that the identity $\Pi_i=V_i$ is only valid under the following additional restrictions: (i) The input angular distribution $|E|^2$ should be identical for all input polarizations in the classical measurements, (ii) the entangled-photon source should be of high quality, i.e., $\Phi_{HV}\approx\Phi_{VH}$, and (iii) the telescope should be a perfect (double) Fourier transformer.

III. EXPERIMENTAL COMPARISON OF CLASSICAL DEPOLARIZATION AND QUANTUM DECOHERENCE

For an experimental verification of the theoretical expectations given above, we have used two different hole arrays, one with a square and one with a hexagonal hole patterning. Both consisted of a 200-nm-thick gold layer on a 0.5-mm-thick glass substrate with a 2-nm-thick bonding layer (of either titanium or chromium) in between. The square array was made with electron-beam lithography and had a lattice spacing of 700 nm and a nominal hole diameter of 200 nm. The hexagonal array was made with ion-beam milling and had a lattice spacing of 886 nm with again a nominal hole diameter of 200 nm. Figure 3 shows measured transmission spectra of the square array (black curve) and the hexagonal array (gray curve). At the experimental wavelength of 813 nm the resonant modes can be assigned to the glass-metal $(\pm1,\pm1)$ and the air-metal (1,0,0), (0,1,0), and (0,0,1) modes for the square and hexagonal array, respectively. The insets in Fig. 4 show scanning electron microscope pictures of the two arrays.

The classical depolarization induced by the hole arrays was measured with the setup shown in Fig. 1. A Ti:sapphire laser beam (wavelength 813 nm) is weakly focused on a 10-μm-diameter pinhole which is positioned at 50 cm in front of a 15-mm focal length lens; the pinhole diffracts the beam enough to produce a nearly plane-wave illumination of the lens. A diaphragm in front of the lens sets the maximum opening angle of the light impinging on the hole array, which is positioned at the focal plane. The transmitted light is recollimated by an identical 15-mm-focal length lens. The far field of the hole-array transmission is then imaged onto a

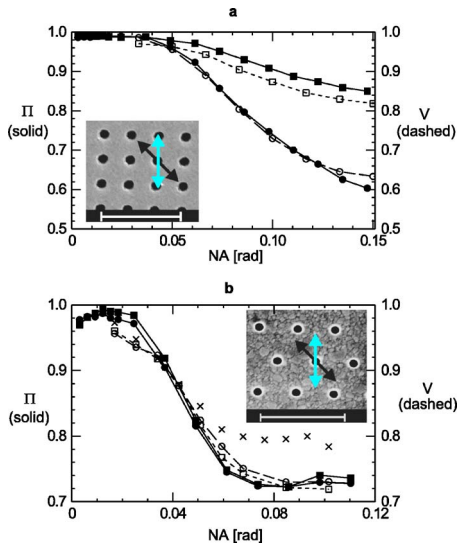

FIG. 4. (Color online) Measured degree of polarization Π_i (solid lines and symbols) and two-photon visibility V_i (dashed lines and open symbols) for (a) the square and (b) the hexagonal array. In both figures the polarization bases are 0° (circles) and 45° (squares). The insets show scanning electron microscope pictures of the arrays (scale bar 2 μm) with arrows indicating the incident polarizations of 0° (light) and 45° (dark). The crosses in (b) are measured with a smaller SPDC aperture in beam 2 (4 mm diameter, equivalent to NA ≈ 0.068 at the array position).

charge-coupled device (CCD) by a relay lens, making the positions on the CCD correspond to angles in the array illumination. The input polarization state is prepared by a combination of polarizer and half-wave plate in front of the first lens. A polarizer behind the second lens constitutes the polarization analyzer. To determine the total power within a given opening angle of the output (and input) beam the intensities per pixel of the CCD image were summed within a circle of corresponding radius. We checked that this software procedure gave the same result as setting the input-beam opening angle with the diaphragm, thus showing that lens abberations are negligible. Further details of the experimental setup are given in Ref. [7].

The measured $\mathcal{D}$ curves (Π_i versus opening angle) for the square (a) and hexagonal (b) array are marked with solid symbols and solid lines in Fig. 4. These results were published before, in Ref. [7]. Circles denote measurements with input polarization along 0° (gray arrows in inset) and squares with input polarization along 45° (black arrows). For the square array, the decrease in Π_{0° upon increasing the numerical aperture (NA) [16] is stronger than that of Π_{45°, because of the $(\pm 1, \pm 1)$ propagation directions of the resonant SPs on this array [7]. For the hexagonal array the equality $\Pi_{0^\circ} = \Pi_{45^\circ}$ holds, as expected from general symmetry arguments [7,12]. The faster decrease of both Π's of the hexagonal array as compared to the square array is caused by the smaller resonance linewidth and therefore larger SP lifetime of the hexagonal array (see Fig. 3) [7]. A more detailed analysis of the measured Π_i's and a comparison with a Fano-type model was published elsewhere [17].

The quantum decoherence was measured with the setup shown in Fig. 2 (see Ref. [8]). A BBO crystal is pumped by a continuous-wave Kr-ion laser beam (wavelength 406.7 nm) in a type-II SPDC scheme. The down-converted photons at the ring crossings are selected by two variable-aperture diaphragms D1 and D2 and further frequency selection was applied by two 10 nm full-width-half-maximum frequency filters centered at the degenerate-frequency point of 813 nm. After passing through polarizers P1 and P2, the photons are detected with avalanche photodiodes 1 and 2. The rate of coincidences is determined with an AND gate (2 ns time window) coupled to a counter. To compensate for birefringence-related walk-off effects we used the standard compensator comprising a half-wave plate and two BBO crystals, each having half the thickness of the generating crystal [14]. Finally, the hole array was positioned at the focus of a one-to-one telescope, with the first lens positioned directly behind the diaphragm D1. For the square and the hexagonal array two 15- and 30-mm focal length lenses were used, respectively; the weaker lenses were used to obtain more accurate data at low NA values. In the absence of hole arrays we regularly obtained coincidence count rates of 40×10^3 s^{-1} with $V_{0^\circ}=99.6\%$ and $V_{45^\circ}=96.0\%$ for a setting of the diaphragm D1 at 4.0 mm and diaphragm D2 at 8.0 mm diameter. Note that even for an empty telescope, on the basis of Eq. (6) we expect a slight decrease of V_{45° with increasing NA, because $\Phi_{HV} \neq \Phi_{VH}$. This is confirmed by measurements: from fully closed (1 mm diameter) to fully open (6 mm) lens apertures we obtain count rates of 2 to 110 $\times 10^3$ s^{-1} and $V_{45^\circ}=98.4\%$ to 91.2%, whereas V_{0° was constant at 99.6%. From this perspective, the spectral detection bandwidth plays a similar role as the angular aperture width; the 10 nm filters were found to be sufficiently narrow as compared to both the spectral width of the SPDC source and the linewidth of the transmission spectra of both arrays.

The measured quantum visibility curves (V_i versus NA) are shown with dashed symbols and dashed lines in Fig. 4, to enable direct comparison with the classical depolarization. An input polarization of 0° is denoted by circles and 45° by squares. Note that the visibility axis has the same scale as the $\mathcal{D}$ axis. By comparing the two sets of curves in Figs. 4(a) and 4(b) we see that there is a good agreement between the visibility V_i and $\mathcal{D}\,\Pi_i$, which confirms the theoretical discussion given above. The consistently slightly lower value of V_{45° as compared to Π_{45° for the square array is probably caused by the limited quality of the source ($V_{45^\circ} < 1$). The slight deviation of the small-NA points for the hexagonal array might be caused by a slight misalignment of the telescope axis c.q. array surface normal with respect to the center of diaphragm D1. Note that in both the classical and the quantum measurements the previously discussed averaging procedure in the measurements of Π_i and V_i was applied because our hexagonal array was not of perfect symmetry [7].

To illustrate a case where the quantum and classical results seem to differ due to a violation of the restrictions discussed earlier, the crosses in Fig. 4(b) show a measurement of V_{45° that was made with diaphragm D2 set at a diameter of 4 mm (equivalent to NA ≈ 68 mrad). Compared to the previously discussed measurement (with D2 at 8 mm diameter), the crossed Π points start to deviate at an NA of approximately 50 mrad and become constant at approximately 70 mrad. Mathematically, the size of the aperture D2 determines

the integration range in Eqs. (10a) and (10b); a smaller integration range leads to a larger visibility. A more conceptual explanation can be given in terms of the Klyshko picture [18]: a photon starting at detector 2 and traveling back along beam 2 is diffracted by diaphragm D2 and, after reflection on the pump-spot mirror, no longer provides for a uniform illumination of the aperture of the lens in beam 1.

IV. CONCLUSIONS

In conclusion, we have reported an experimental comparison between the classical depolarization and the quantum decoherence induced by subwavelength metal hole arrays of square and hexagonal symmetry. We find that there is an identity relation between two suitable measures of these effects, for ideally prepared input sources. This identity relation can theoretically be completely expressed in the hole array transmission tensor. Deviations show up if the input sources are not polarization isotropic or have insufficient spatial coherence.

APPENDIX: DEGREE OF POLARIZATION FOR NONPERFECT ARRAYS

To be able to characterize the depolarization induced by square and hexagonal arrays which have some (slight) symmetry deformations, we extend the definition of the degree of polarization ($\mathcal{D}$) as follows. In the simplest case, we can define a measure for the depolarization of a system in terms of the Stokes vector of the output light:

$$\Pi_i \equiv \left(\frac{S_i}{S_0}\right)_{out} = \frac{P_\parallel - P_\perp}{P_\parallel + P_\perp}, \tag{A1}$$

for a fully polarized input $S_{in}=(1,\delta_{i1},\delta_{i2},\delta_{i3})$ $(i=1,\ 2,\ 3)$. The Π_i so-defined are only equal to the $\mathcal{D}$ of the output light if the output Stokes vector contains the same two zero components as the input Stokes vector, i.e., if the medium can be described by a diagonal Mueller matrix.

A more generally usable measure for depolarization can be defined by symmetrizing Π_i with respect to the input Stokes vectors:

$$\Pi_i^{av} \equiv \frac{S_i^+ - S_i^-}{S_0^+ + S_0^-} = \frac{P_\parallel^+ + P_\parallel^- - (P_\perp^+ + P_\perp^-)}{P_\parallel^+ + P_\perp^+ + P_\parallel^- + P_\perp^-} = \frac{M_{ii}}{M_{00}}, \tag{A2}$$

where $S_i^\pm \equiv S_i^{out}$ for $S^{in}=(1,\pm\delta_{i1},\pm\delta_{i2},\pm\delta_{i3})$. This expression is exactly equal to the respective diagonal Mueller-matrix element M_{ii}, normalized to M_{00}, as indicated by the last equality in Eq. (A2). If the nondiagonal elements of the Mueller matrix are small compared to the diagonal elements, Π_i^{av} is also approximately equal to the average of the $\mathcal{D}$'s of the output light for both input Stokes vectors. This follows from a Taylor expansion of the $\mathcal{D}$'s via

$$\begin{aligned}\frac{\mathcal{D}^+ + \mathcal{D}^-}{2} &= \frac{1}{2}\left(\frac{\sqrt{(M_{10}+M_{1i})^2+(M_{20}+M_{2i})^2+(M_{30}+M_{3i})^2}}{M_{00}+M_{0i}}\right.\\ &\left.+\frac{\sqrt{(M_{10}-M_{1i})^2+(M_{20}-M_{2i})^2+(M_{30}-M_{3i})^2}}{M_{00}-M_{0i}}\right)\\ &\approx \frac{M_{ii}}{M_{00}}\left(1+\frac{\sum_{j\neq i}^{j\neq 0} M_{j0}^2+M_{ji}^2}{2M_{ii}^2}-\frac{M_{0i}M_{i0}}{M_{00}M_{ii}}+\frac{M_{0i}^2}{M_{00}^2}\right).\end{aligned} \tag{A3}$$

The $\mathcal{D}^+$ and $\mathcal{D}^-$ are each sensitive to first-order in the relative strength of the off-diagonal elements M_{ij}. However, as the respective first-order terms differ in sign, the averaging removes these terms to leave only terms of second-order and higher. The final expression is accurate for $M_{ij}\ll M_{ii}$ (for $i\neq j$). (Note, $M_{00}\geqslant M_{ii}$ always.) In the main text we will use Π^{av} only, and drop the "*av*" superscript label.

[1] T. W. Ebbesen, H. J. Lezec, H. F. Ghaemi, T. Thio, and P. A. Wolff, Nature (London) **391**, 667 (1998).

[2] H. Raether, *Surface Plasmons* (Springer, Berlin, 1988).

[3] J. Elliott, I. I. Smolyaninov, N. I. Zheludev, and A. V. Zayats, Opt. Lett. **29**, 1414 (2004).

[4] K. J. K. Koerkamp, S. Enoch, F. B. Segerink, N. F. van Hulst, and L. Kuipers, Phys. Rev. Lett. **92**, 183901 (2004).

[5] R. Gordon, A. G. Brolo, A. McKinnon, A. Rajora, B. Leathem, and K. L. Kavanagh, Phys. Rev. Lett. **92**, 037401 (2004). Unfortunately, the authors employ the word depolarization in an improper way by using it to describe a change of one spatially *uniform* polarization into another spatially *uniform* polarization.

[6] E. Altewischer, M. P. van Exter, and J. P. Woerdman, J. Opt. Soc. Am. B **20**, 1927 (2003).

[7] E. Altewischer, M. P. van Exter, and J. P. Woerdman, Opt. Lett. **30**, 90 (2005).

[8] E. Altewischer, M. P. van Exter, and J. P. Woerdman, Nature (London) **418**, 304 (2002).

[9] E. Moreno, F. J. Garcia-Vidal, D. Erni, J. I. Cirac, and L. Martin-Moreno, Phys. Rev. Lett. **92**, 236801 (2004).

[10] R. M. A. Azzam and N. M. Bashara, *Ellipsometry and Polarized Light* (North-Holland, Amsterdam, 1987).

[11] F. Le Roy-Brehonnet and B. Le Jeune, Prog. Quantum Electron. **21**, 109 (1997).

[12] C. Genet, E. Altewischer, M. P. van Exter, and J. P. Woerdman, Phys. Rev. B **71**, 033409 (2005).

[13] M. H. Rubin, D. N. Klyshko, Y. H. Shih, and A. V. Sergienko, Phys. Rev. A **50**, 5122 (1994).

[14] P. G. Kwiat, K. Mattle, H. Weinfurter, A. Zeilinger, A. V. Sergienko, and Y. Shih, Phys. Rev. Lett. **75**, 4337 (1995).

[15] D. N. Klyshko, *Photons and Non Linear Optics* (Gordon and Breach, New York, 1980).

[16] M. Born and E. Wolf, *Principles of Optics* (Pergamon, Oxford, 1980).

[17] E. Altewischer, M. P. van Exter, and J. P. Woerdman, J. Opt. Soc. Am. B (to be published).

[18] D. N. Klyshko, Sov. Phys. JETP **67**, 1131 (1988).